ORIGINAL

CrossMark

A 3-D numerical simulation of non-Newtonian blood flow through femoral artery bifurcation with a moderate arteriosclerosis: investigating Newtonian/non-Newtonian flow and its effects on elastic vessel walls

Mohammad Hassan Amiri[1] · Ahmad Keshavarzi[1] · Arash Karimipour[2] · Mehdi Bahiraei[3] · Marjan Goodarzi[4] · J. A. Esfahani[5]

Abstract

In this study, a fluid-structure interaction (FSI) simulation of the blood flow in the femoral artery with a small occlusion is presented. For a more accurate simulation of the real conditions, computerized tomography (CT) scan was used to obtain a 3-D model of leg blood vessels, while the vessel was modeled as an isotropic elastic wall. By assuming a heartbeat period of 0.5 s, the inlet condition was considered as a time-dependent pulse using a non-Newtonian flow model. Blood flow was assumed nonlinear and incompressible, and Carreau model was used for blood rheological model.

By considering unstable blood flow at the inlet, the involved hemodynamic parameters are velocity profile, vortices shapes, pressure drop, and streamlines. Furthermore, to determine the relationship between flow geometry and the vascular wall, wall shear stress (WSS) was calculated.

By taking the real geometry of the vessel and fluidity of blood into account, comparison of computational results indicated a significant difference in velocity distribution and shear stress depending on whether the fluid-structure interaction is considered Newtonian or non-Newtonian. The results showed that employing Newtonian models for the blood flow does not lead to promising results at occluded areas and beyond them.

✉ Marjan Goodarzi
marjan.goodarzi@tdtu.edu.vn

1 Department of Mechanical Engineering,
Khomeinishahr Branch, Islamic Azad University,
Khomeinishahr, Iran

2 Department of Mechanical Engineering, Najafabad Branch
Islamic Azad University, Najafabad, Iran

3 Department of Mechanical Engineering
Kermanshah University of Technology,
Kermanshah, Iran

4 Sustainable Management of Natural Resources
and Environment Research Group,
Faculty of Environment and Labour Safety
Ton Duc Thang University,
Ho Chi Minh City, Vietnam

5 Department of Mechanical Engineering,
Faculty of Engineering, Ferdowsi University of Mashhad,
P.O. Box 91775-1111, Mashhad, Iran

Nomenclature

X, Y, Z	Coordinates
U_f	Velocity vector (m/s)
ρ_f	Blood density (kg/m^3)
σ_f	Stress tensor
p	Blood pressure (Pa)
I	Identity matrix
$\eta_f(\dot{\gamma})$	Blood viscosity (Ns/m^2)
$\dot{\gamma}$	Shear strain
η_{0f}	Zero strain viscosity ($Pa.\,s$)
$\eta_{\infty f}$	Infinite strain viscosity ($Pa.\,s$)
n	Empirical exponent
λ_f	Time constant (s)
E	Young module (N/m^2)
ν	Poisson ratio
ρ_s	Artery density (kg/m^3)
L_s	Artery wall displacement (m)
d_i^f	Fluid displacement at FSI (m)

d_i^s Artery displacement at FSI (m)

m Normal vector at FSI

t Time (s)

1 Introduction

Cardiovascular diseases (CVDs) are among the leading causes of death, killing more than 17.3 million people annually; a number that is expected to rise to 23.6 million by 2030. More than 30% of fatalities in 2008 were due to CVDs, 80% of which occurring in underdeveloped and developing countries. In 2011, CVDs killed 787,000 people in the U.S. that are accounted for one-third of the total deaths in this country [1].

Different types of CVDs include infarction (hemorrhagic and ischemic), thrombus and aneurysm [2]. An essential type of CVDs is known as peripheral artery disease (PAD). Limited blood flow in any part of the body can cause serious problems which ultimately affects the heart. PAD is a common circulatory problem which causes decreased blood flow to the vessels of lower extremities and is caused by plaque accumulation (made up of cholesterol and other fatty materials). The deposition of these materials is known as atherosclerosis. Smokers or diabetes have a higher risk of developing PAD. Moreover, PAD is more prevalent in patients aged 50 to 69. Generally, 20% of men and 16% of women over 65 are diagnosed with this disease [3]. If not treated in time, PAD can lead to heart attacks or strokes. The risk of heart attack or stroke in people who are diagnosed with PAD but not undergoing treatment is 6 to 7 times more than healthy individuals [4]. Blood Rheological behavior in large blood vessels can be assumed Newtonian. However, in small vessels, this is not a correct assumption [5]. Human blood is

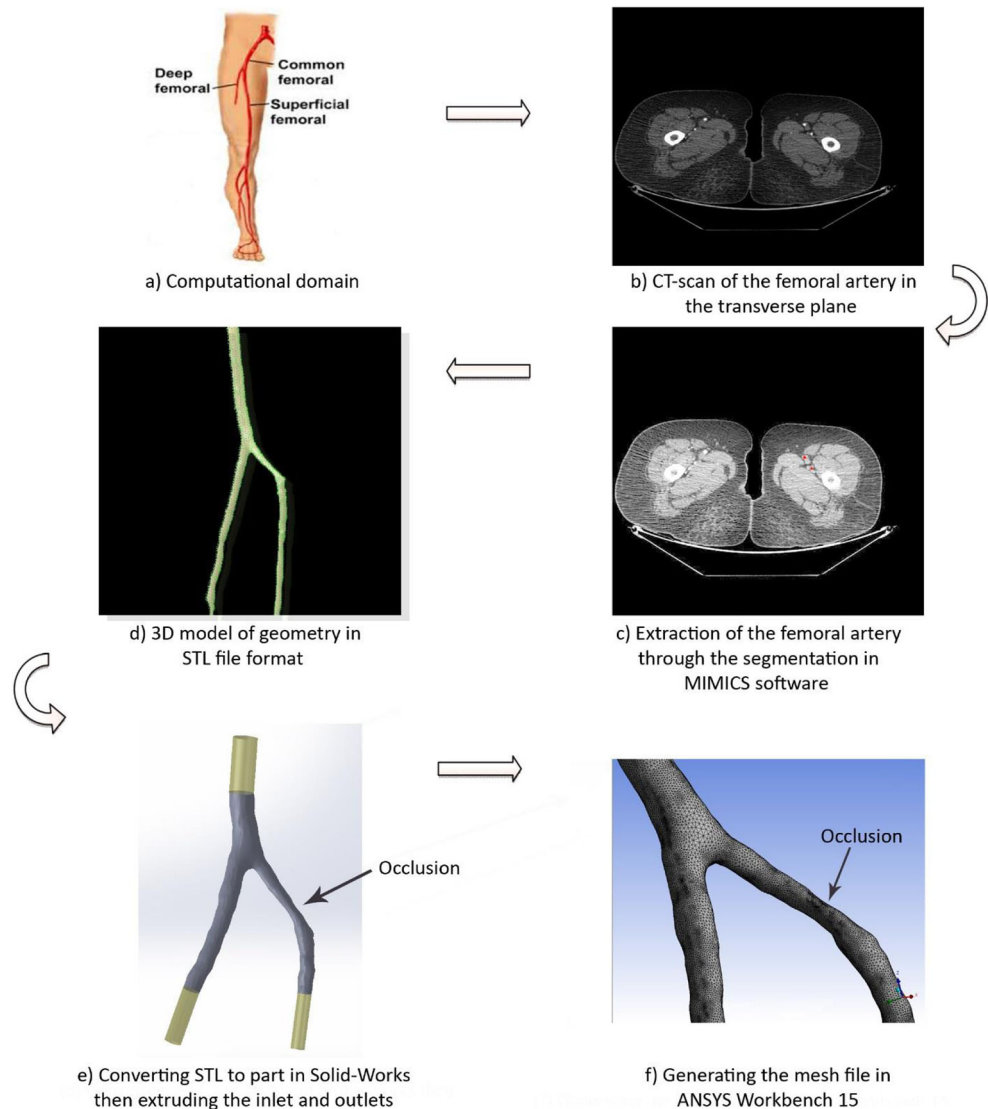**Figure 1** The steps taken for preparation of the real 3D model from CT-Scan images

a) Computational domain

b) CT-scan of the femoral artery in the transverse plane

c) Extraction of the femoral artery through the segmentation in MIMICS software

d) 3D model of geometry in STL file format

e) Converting STL to part in Solid-Works then extruding the inlet and outlets

f) Generating the mesh file in ANSYS Workbench 15

Table 1 Coefficients for non-Newtonian Carreau model [19]

| η_{0f}	$\eta_{\infty f}$	λ_f	n
0.056 (Pa.s)	0.00345 (Pa.s)	0.313 (s)	0.357

composed of erythrocytes, leucocytes, and thrombocytes while its flow through vessels can be considered pulsatile and non-Newtonian in an elastic tube.

Although there have been researches on the simplified models of vessels in order to investigate occlusion and its effects on blood flow, they are generally based on the assumption of symmetry and ideal geometries. Meanwhile, by considering a Newtonian flow through a cylindrical tube model, Young [6] assumed a small axial occlusion and investigated occlusion growth on pressure distribution, wall shear stress and its effects. Lee and Fung [7] also investigated occlusion in the cylindrical model and reported numerical results on pressure distribution, velocity and shear stress in Reynolds numbers of 0 to 25. They concluded that geometry, as well as Reynolds number, profoundly affects the results. Morgan and Young [8] studied large and small occlusions of Newtonian blood flow in an asymmetric vessel in low Reynolds numbers and presented velocity distribution, pressure drop, and wall shear stress. By comparing the changes in models, they concluded that there is a correlation between results and their geometries. Later on, studies were conducted

on asymmetric geometries, the conditions of which were closer to a real blood vessel. For instance, Azuma and Fukushima [9] studied both symmetric and asymmetric occluded, steady Newtonian flows and investigated the effects of different Reynolds numbers and occlusion. Liu and Wang [10] selected conical geometry for their model and used the Newtonian fluid as well as inelastic asymmetric models to investigate wall shear stress and their effects on damaging vessel walls in different conditions. The most research conducted by then described blood rheology as Newtonian. However, experimental observations suggested non-Newtonian behavior for blood [11, 12]. The experimental results expanded the researches on non-Newtonian behavior. Mandel [13] used conical vessel geometry, time-dependent model and the power-law fluid model to obtain velocity profile, volumetric flow rate and wall shear stress. In line with these investigations, researchers mostly focused their attention on specific body vessels which were normalized with major body vessels, e.g., Aorta and Carotid arteries. Assuming a non-Newtonian flow and using power-law fluid model, Obidowski and Jozwik [14] used a sophisticated, normalized model of vertebral artery to investigate velocity profiles in different branches and bifurcations. Wang and et al. [15] used a Newtonian blood model in a coronary artery to investigate the effect of different geometry angles on the flow, artery wall, and pressure variations. They showed that changes in geometry affect wall shear stress the most; while having insignificant effects on velocity as well as

Fig. 2 Model geometry: **a** fluid domain, **b** structure domain and **c** coupled domain
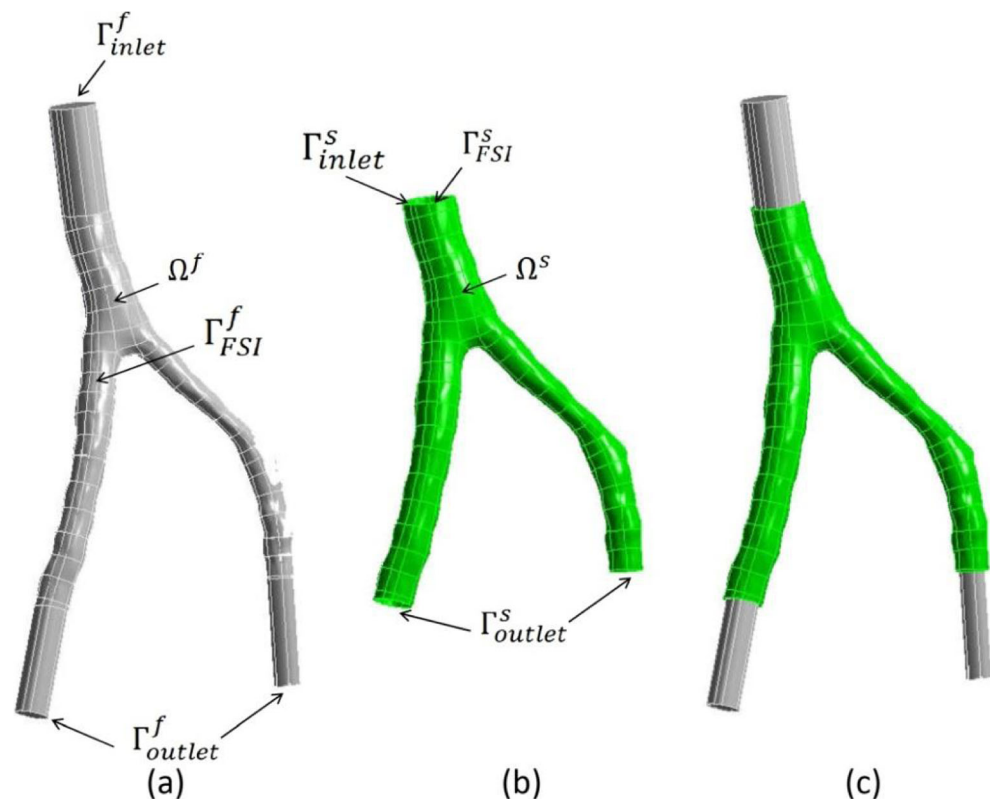
pressure fields. Recently, real artery models have been made possible through CT-scan and MR-based imaging in order to achieve more accurate results which have attracted researchers' attention. Jalali et al. [16] used pulsatile, non-Newtonian flow model based on CT-scan images to investigate non-Newtonian fluid and wall shear stress effects.

The femoral artery is a continuation of the external iliac artery in the thigh and the main arterial supply to the lower limb. Femoral artery bifurcation in a leg is among the most crucial body vessels which assume different angles in different individuals. The bifurcation splits the main artery into two, one of which supplies blood to the thighs and called deep femoral artery and the other supplies blood to the knee and the lower parts of the leg and called superficial femoral artery.

The present study aims to investigate unsteady blood flow in order to determine the affecting hemodynamic parameters for the bifurcation model of the real femoral artery, based on CT-scan images. In the following sections, the one-way coupling is used to investigate flow effects on the vessel wall. All simulations were done in ANSYS 15 commercial software package in FSI mode, coupling FLUENT with the Transient Structural mode. Blood flow model in this simulation was assumed incompressible and non-Newtonian.

2 Preparing a model based on CT-scan

As demonstrated in Fig. 1, the domain of study was focused on artery CT-scan images of a 57-year old woman with small vessel occlusions. The single-matrix scanner was used in a helical mode with a field of view (FOV) of 500-mm, 100 kV peak, and 550 mA, and it included 1052 continuous images of 1.25 mm thickness. The scanning was started from the abdomen area and was finished at
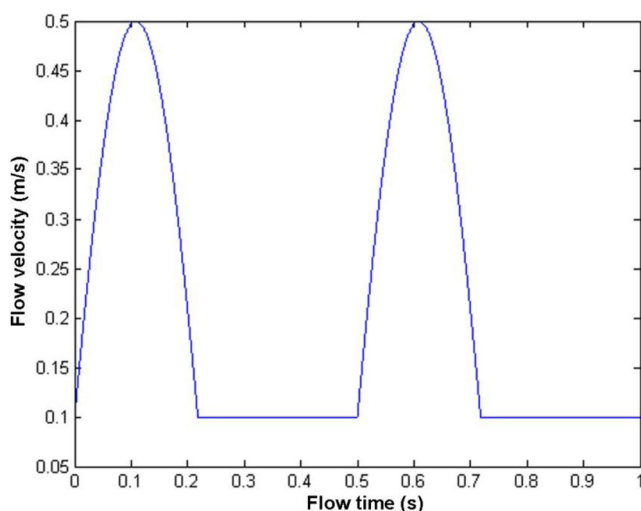
the foot. The 2-D CT DICOM images in 3 directions (x-y-z) were imported to the MIMICS commercial package for reconstruction of the domain to 3-D geometry. The output file was a Standard Tessellation Language (STL) file format which was converted to a 3-D part file using Solid-Works 2013. The inlet and outlet of vessels in a three-dimensional model was cut using the Cut-extrude feature in Solid-Works 2013, and the solid wall was defined as a shell surrounding the model environment.
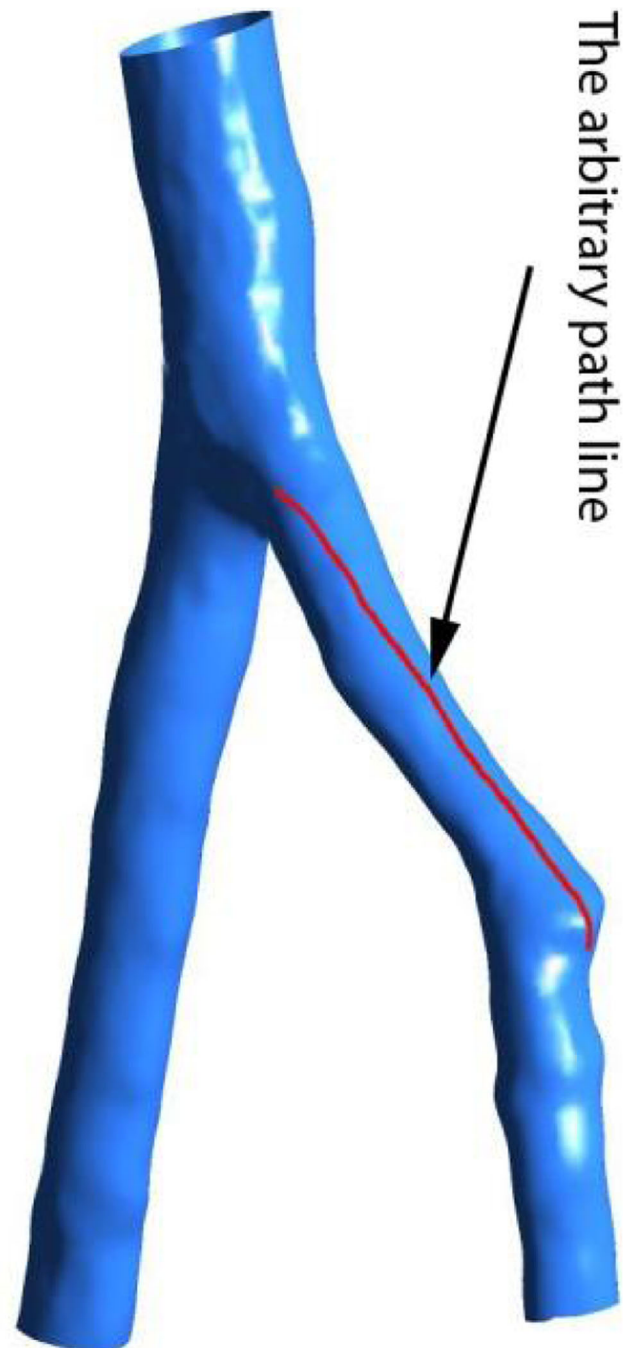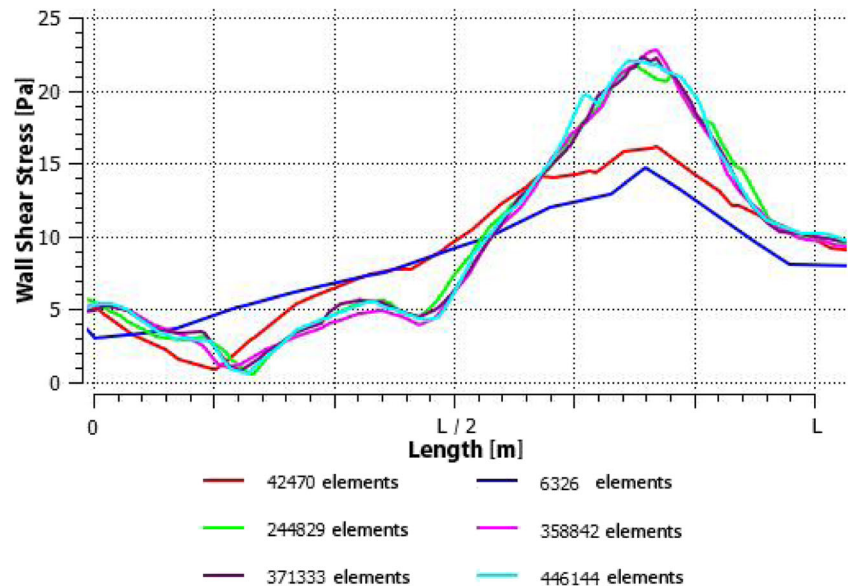

Figure 4 The absolute path line on the model for grid independence study

Figure 3 Inlet velocity profile [19]

Figure 5 Comparison of wall shear stress on the selected path line with the different number of meshes

Ultimately, the final file was prepared in STEP format and was imported into ANSYS Workbench 15. It was then imported into the meshing module for meshing purposes, and then it was imported into the FLUENT software.

3 Governing equations

In the present study, blood was assumed as an incompressible, non-Newtonian fluid in a laminar regime with zero gravity [17]. The governing equations which include Navier-Stokes equations for both conservations of mass and momentum are as follows [17]:

$$\nabla . U_f = 0 \tag{1}$$

$$\rho_f \left[\frac{\partial U_f}{\partial_t} + \left(U_f . \nabla \right) U_f \right] = \nabla . \sigma_f \tag{2}$$
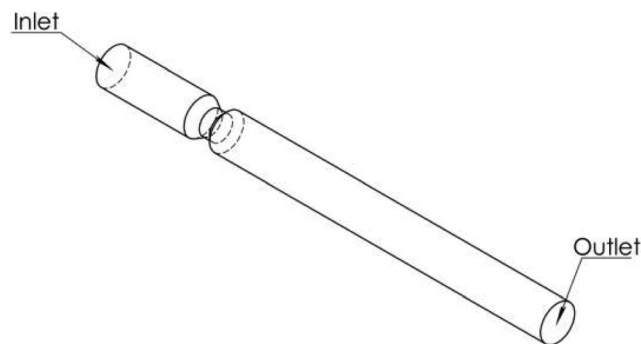

Fig. 6 The studied model by Chan et al. [20]

Where the blood density is 1060 kg/m^2 and the total stress tensor defined as:

$$\sigma_f = -pI + \eta_f \left(\dot{\gamma} \right) \left[\nabla U_f + \left(\nabla U_f \right)^T \right] \tag{3}$$

The fluid shear strain rate is defined as:

$$\dot{\gamma} = \sqrt{2 \, tra \left[\frac{1}{2} \left(\nabla U_f + \left(\nabla U_f \right)^T \right) \right]^2} \tag{4}$$

The blood viscosity is obtained using the non-Newtonian Carreau model [18]

$$\frac{\eta_f \left(\dot{\gamma} \right) - \eta_{\infty f}}{\eta_{0f} - \eta_{\infty f}} = \left[1 + \left(\lambda_f \dot{\gamma} \right)^2 \right]^{\frac{(n-1)}{2}} \tag{5}$$
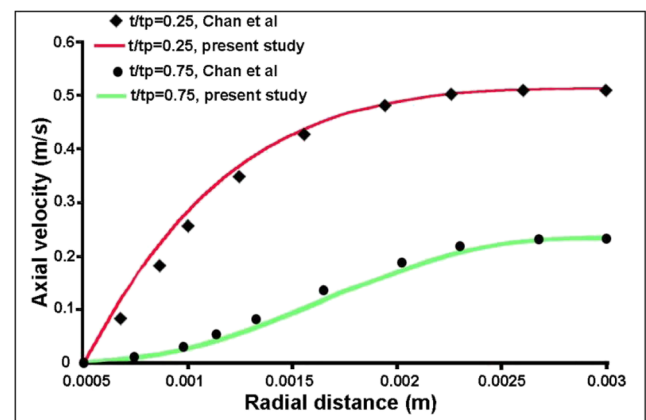

Fig. 7 Comparison of axial velocity between the results of present study and that of Chan et al. [20] at $z^* = 4.3$. (z^* is the normalized distance from the center of stenosis by diameter)
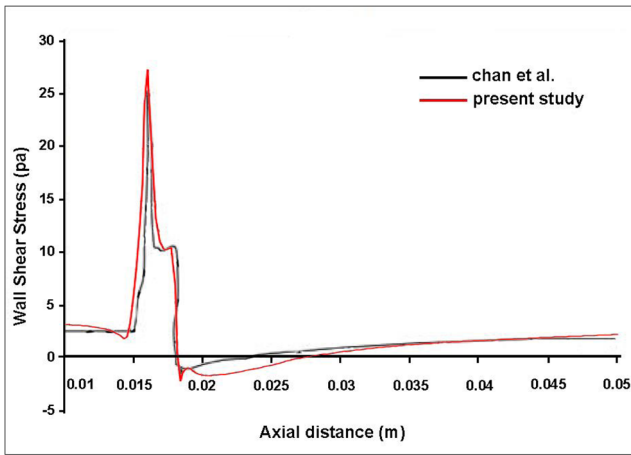
Fig. 8 Comparison of shear stress variations between the results of the present study and that of Chan et al. [20] at T = 0.25

Constants in the above relations are shown in Table 1. Wall thickness is considered equal to 0.5 mm.

For an isotropic model of the artery elastic wall, Young's Module and Poisson's Ratio can be selected as $E = 1.08\ MPa$ and $\nu = 0.45$, respectively. Elastic equation of motion is:

$$\rho_s \frac{\partial^2 L_s}{\partial t^2} = \nabla . \sigma_s \qquad (6)$$

Where the density value is assumed to be: $\rho_s = 1200\ kg/m^2$

The fluid and solid equations were separately discussed up to now. However, conditions should be added to the problem in order to describe the fluid-structure interactions. This is also known as fluid-structure interaction (FSI). Therefore, cinematic and dynamic compatibility conditions should be met at the fluid-structure interface boundary. The cinematic compatibility which states non-slip condition at the wall is defined as:

$$d_i^f = d_i^s \qquad (7)$$

$$\frac{\partial d_i^f}{\partial t} = \frac{\partial d_i^s}{\partial t} \qquad (8)$$

The dynamic compatibility condition can be defined as:

$$m_j \tau_{ij}^f = m_j \tau_{ij}^s \qquad (9)$$

The solution first solves the governing equations of the fluid and solid fields separately and then transfers the resulting forces obtained from the fluid field at the FSI to the solid field.

4 Boundary conditions

Fluid domain, as depicted in Fig. 2, includes the inlet $\left(\Gamma_{inlet}^f\right)$, outlet $\left(\Gamma_{outlet}^f\right)$ and fluid-structure interface $\left(\Gamma_{FSI}^s\right)$. The imposed boundary condition at the inlet was a time-dependent velocity profile as demonstrated in Fig. 3 which can be described by the following equation where a complete cycle lasts for 0.5 s [19]:

$$v_{inlet}(t) = \begin{cases} 0.5\sin\left[4\pi(t + 0.0160236)\right] & : 0.5n < t \leq 0.5n + 0.218 \\ 0.1 & : 0.5n + 0.218 < t \leq 0.5(n+1) \end{cases} \qquad (10)$$

The average blood pressure of a healthy individual −100 mmHg (13,332 Pa)- was applied at the outlets as constant pressure. For the fluid-structure interface surface (Γ_{FSI}^f), the non-slip condition was applied as the boundary condition.

The structured domain (Ω^s) was divided into three sections: inlet $\left(\Gamma_{inlet}^s\right)$, outlet $\left(\Gamma_{outlet}^s\right)$ and the fluid-structure contact surface $\left(\Gamma_{FSI}^s\right)$. The inlet and outlet cross-sections were assumed static and had no displacements. The contacts surfaces Γ_{FSI}^f and Γ_{FSI}^s correlate the structure domain with the fluid domain. The displacements of fluid and structure are assumed to be equal at their interface. The fluid surface forces at the interface boundary also act as the surface loads applied to the structure domain.

5 Numerical methods and grid independence study

ANSYS 15 commercial package was used to solve and couple the fluid and structure governing equations. One-way coupling method was utilized in this study since the wall displacement in the structure domain is negligible and do not have any significant effects on the fluid domain as compared with the effects of boundary conditions. Considering that the model is a realization of the real world samples, no specific dimensions may be attributed to it. As

Table 2 Selected time frames

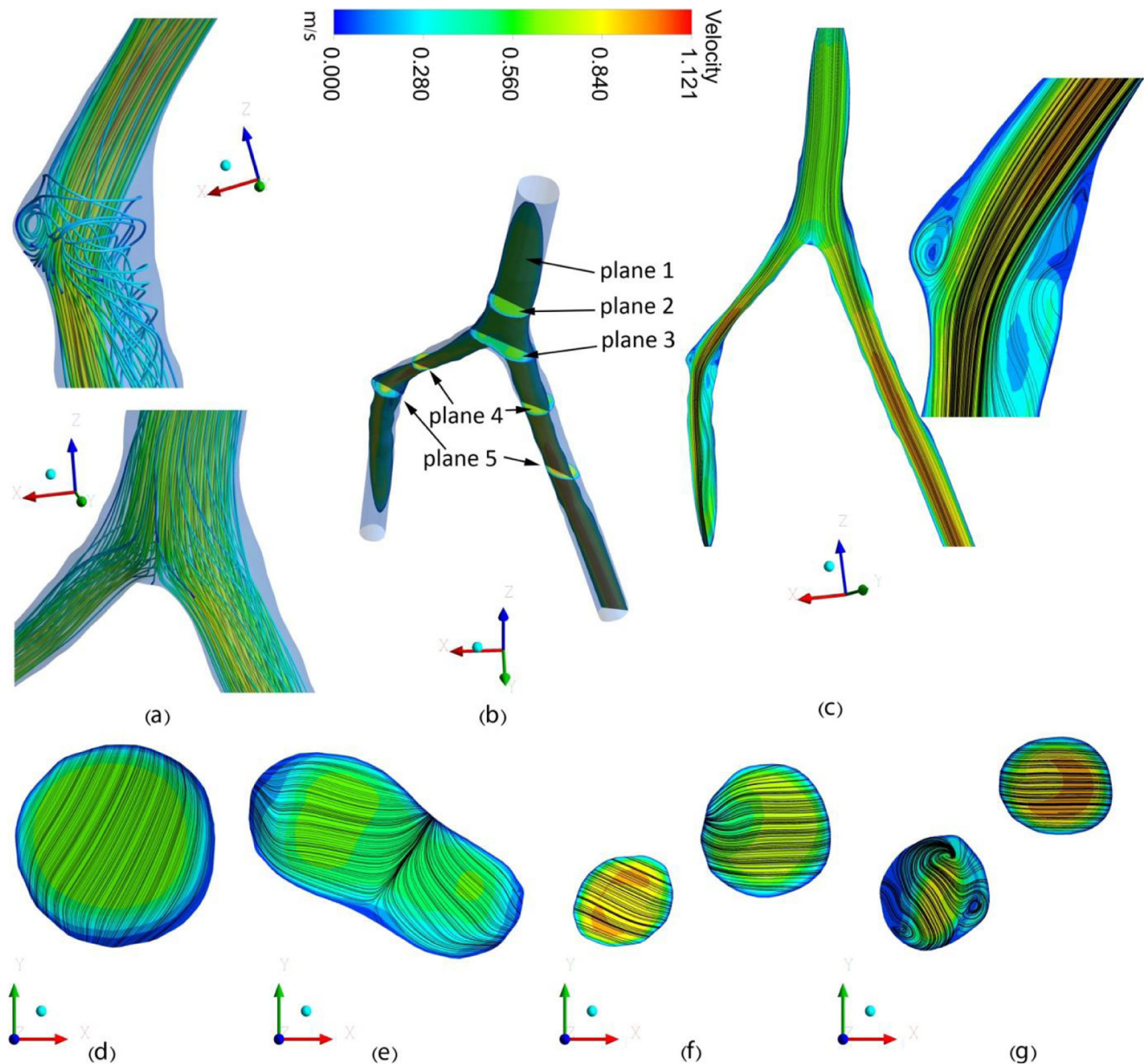| Inlet velocity	Midway-systolic	Maximum flow	Midway-diastolic	Minimum flow	Minimum flow	Minimum flow
$T = {}^t/_{tp}$	$T_1 = 0.1$	$T_2 = 0.2$	$T_3 = 0.3$	$T_4 = 0.4$	$T_5 = 0.7$	$T_6 = 1$

Fig. 9 2-D and 3-D contours and streamlines at the time of maximum flow (t$_2$). (a) 3-D streamlines, (b) surface locations, (c) contour and streamlines of plane 1 (c), plane 2 (d), plane 3 (e), plane 4 (f) and plane 5 (g)

illustrated in Fig. 1d, the fluid and structure solution domains meshed with 371,333 and 169,540 number of hexagonal elements, respectively. To prove the grid independency, various analysis based on the same conditions were used in the different number of elements. By comparing stress changes and streamlines at different locations, it was observed that increasing grid elements only increases memory usage and solving time and it has no significant effects on the results. To present this result, wall shear stress was investigated on an arbitrary path line on the stenosed branch (Fig. 4). The number of grid elements was investigated in 6 different conditions. As is depicted

in Fig. 5, the increase in the number of elements has insignificant influences on wall shear stress.

ANSYS FLUENT commercial software -which is based on the control volume method-, was used in this study to simulate blood flow. Due to model complexity and a large number of elements as well as to increase computational accuracy, the 3ddp version of the software was utilized. Moreover, to reduce the solving time, each pulse was divided into 50 equal time intervals. The convergence criterion for continuity and velocity equations was selected as 10^{-4}. The SIMPLE algorithm was used for coupling the pressure, and momentum equations and under-relaxation

factors for these equations were selected as 0.7 and 0.3, respectively [16].

6 Numerical validation

To validate the solution method, the results of the present study were compared with the numerical findings of Chan et al. [20]. In that work, authors have studied pulsatile blood flow in occluded vessels (Fig. 6) and used 4.3 ± 2.6 mL/s sinusoidal volumetric flow with a period of 0.345 s. A constant pressure of 4140 Pa was considered as outlet boundary condition. The obtained axial velocity profile and wall shear stress using the Carreau model are demonstrated against previous studies in Figs. 7 and 8. As can be observed in these figures, there is a good agreement between the results of the present study and that of Chan et al. [20].

7 Results and discussion

The effects of blood flow, as well as artery occlusion on flow velocity, wall shear stress and its effects on artery wall deformation were investigated in this study. For this purpose, a real model of a femoral bifurcation was prepared using CT-Scan images of a 57-year-old woman. According to the authors' knowledge, this study was one of the first CFD investigations on the real geometry of a femoral stenosis artery on Bifurcation model.

Computational domain along the artery is limited to a length of $L = 37 mm$. Also, $t = 0.01 s$ and $t_P = 0.5 s$ are considered as time-step and total simulation solving time, respectively. According to the calculations, reducing the time-step only increases solving time calculations and does not improve the results.

Table 2 shows different simulation solving times, where T is the ratio of time in seconds (t) to the period of the flow cycle (t_P).

The 3-D streamlines in the two critical areas are demonstrated in Fig. 9a. The figure suggests that the effects of even small occlusions on the flow are higher than that of artery bifurcation. This result is similar to changes which happen in the shape of the flow, velocity and its effects on the wall of the vessel.

Figure 9b shows the contour planes position, the plane 1 that approximately intersects the middle of artery geometry. It should be noted that as the modeled geometry is asymmetric and 3-D, an approximate plane was chosen.

According to Fig. 9c, due to asymmetric geometry and flow velocity increase at the occlusion location, vortices
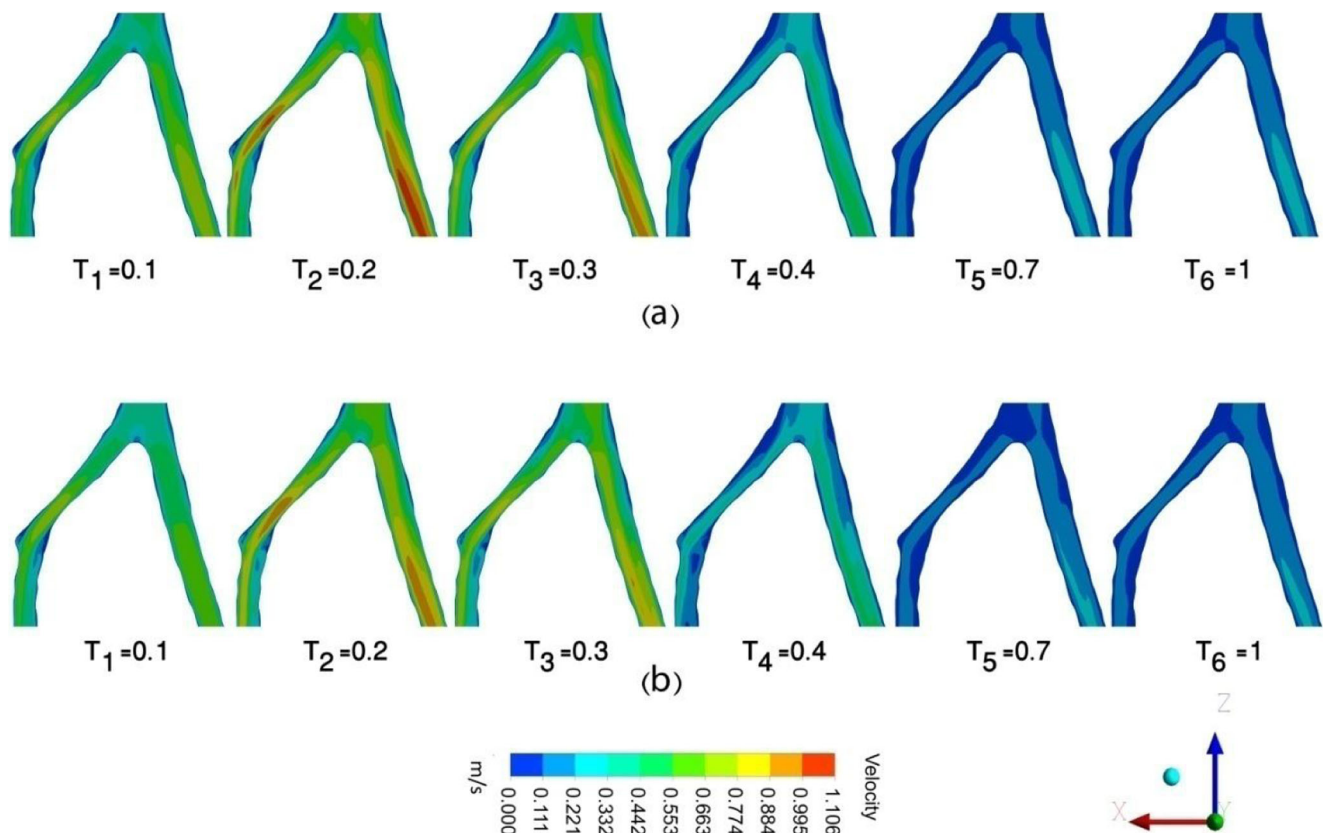

Figure 10 Velocity distribution on the middle plane and at the selected times; **a** non-Newtonian model and **b** Newtonian model
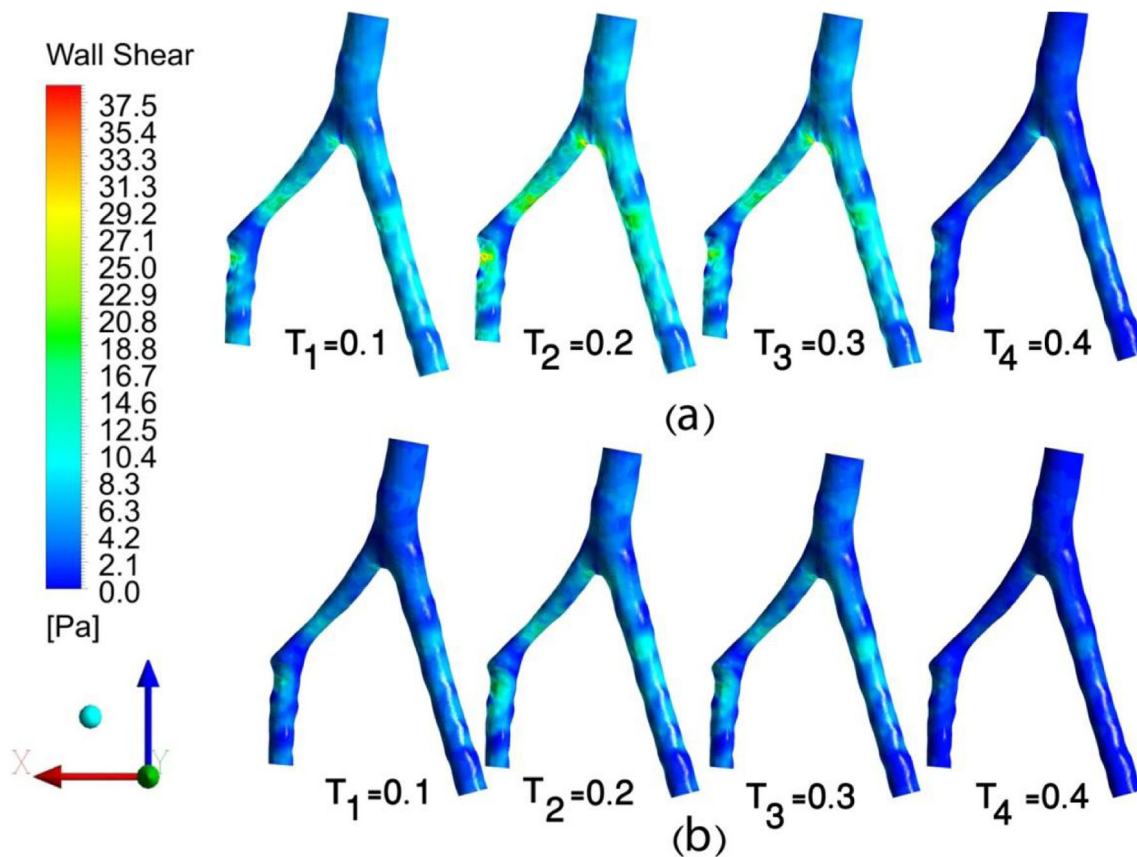
Figure 11 Distribution of wall shear stress for **a** non-Newtonian model and **b** Newtonian model at specific times

are created in the blood flow. Figure 9d to g represent the secondary flow streamlines overlaid onto axial velocity contour on selected cross-sections describe the flow phenomena in more details. The flow disturbance, as well as velocity increase as the flow and, reaches occlusion and bifurcation. Such high variations in the flow properties can profoundly affect the artery wall. The increase in flow velocity is evident at the center of occlusion due to the reduced cross-section. Figure 9e demonstrates the flow before the artery bifurcation. Comparison of Fig. 9d and e reveals that as streamlines near the bifurcation, they reform to two separate branches. The effects of occlusion and geometry changes on the blood flow after the occlusion are depicted in Fig. 9g which shows notable changes in the shape of the flow, velocity and its effects on the wall of the vessel and also the development of vortices and disturbances in the flow.

Velocity distribution contours of plane 1 (Fig. 9b) which approximately intersect the middle of artery geometry, are demonstrated in Fig. 10 at specified times for both Newtonian and non-Newtonian fluids. According to the figure, velocity distributions, as well as the resulting disturbances, are significantly affected by assuming the blood as a non-Newtonian fluid.

Velocity distribution at the inlet -which is larger in diameter-, remains nearly identical for both Newtonian and non-Newtonian assumptions; however, they are different at the occlusion area and after it, such that the maximum velocity in the non-Newtonian model is 12% greater than that of the Newtonian model. Moreover, disturbance effects after the occlusion are more significant in the Newtonian model.

Wall shear stress plays a significant role in the artery wall behavior. In the previous studies, arbitrary paths were commonly used for investigating and analyzing the shear stress [21]. However, this assumption is only applicable in simple/ normalized models and may not be extended to the artery real 3-D model due to its natural complexities. Regarding the previous sentence, 3-D wall shear stress contours at the selected times are represented in Fig. 11.

Wall shear stress is directly related to the velocity variations close to the wall, and geometry variations cause these variations. In other words, any changes in the artery geometry affect the blood flow. At locations where flow enters a narrow inlet, which may also be an occlusion, or where a bifurcation occurs shear stress increases. According to Fig. 11 and the comparison made between Newtonian and non-Newtonian flows, the maximum shear
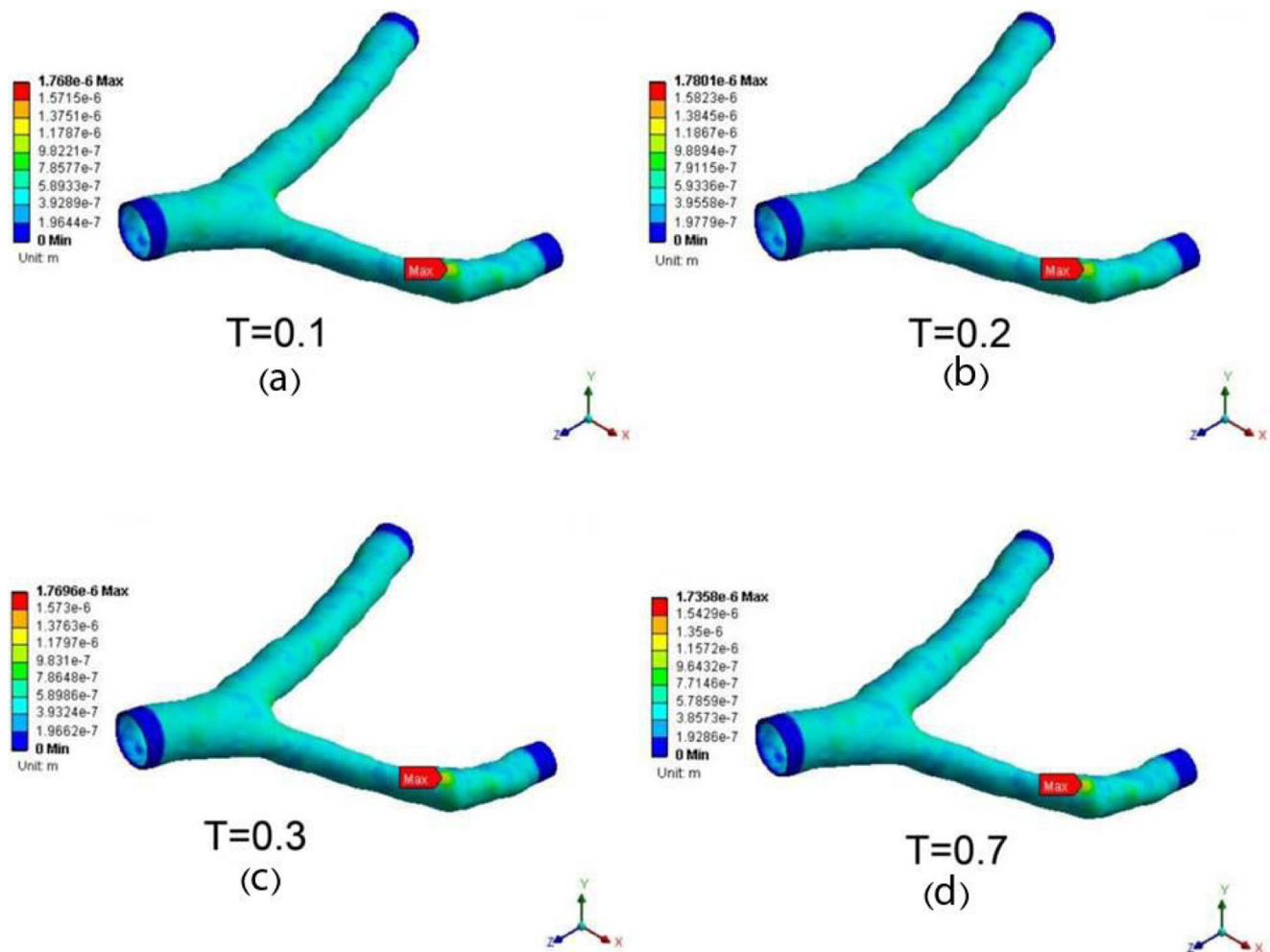
Figure 12 Artery wall displacement contours at four specified times

stress occurs at the aforementioned critical areas. Based on the selected models, the variations of velocity in the Newtonian model are less than the non-Newtonian case, and the effect of this phenomenon is shown as the wall shear stress in Fig. 11. Despite a 12% difference in the velocity, there is a 50% difference between the values of maximum wall shear stress in two models. This difference proves that the assumption of the Newtonian model in the occluded, narrow arteries, or at the bifurcations cannot deliver promising results.Fry [22] showed that wall shear stresses of 40 Pascal or higher might damage artery endothelial cells [22]. In another study, Ramstack and et al. [23] showed that the increase in wall shear stress could lead to endothelial cell rupture which increases the chance of thrombus formation. The result of the present study showed that the maximum wall shear stress is more like to occur at or right after the occlusions. Since 40 Pa is assumed as the critical value, according to Fig. 9c, the wall deformation caused by blood flow at the occlusion may be regarded as a sign of artery thrombus.

Total artery wall displacement caused by fluid interactions at specific times is demonstrated in Fig. 12. Systolic pressure (the increase of flow to maximum), diastolic pressure (decrease of flow from maximum) and the minimum flow pressures of pulsatile heartbeats in the cardiac cycle are demonstrated in Fig. 12a to d, respectively.

The artery structure can freely move in all directions. Since fixed supports are extended over the artery inlet and outlet walls, maximum displacements occur normal to the flow direction. A comparison of Fig. 12a and b reveals that the displacement of the vessel wall is comparable with the values shown in the legend; in midway systole and midway diastole.

The results also indicated that maximum wall displacement occurs after the occlusion, which may cause further deformations in the artery over time, leaving undesired effects on the downstream flow. The concluded results in this study justify the deformations after the occlusion and show that small artery occlusions can leave severe effects on the artery geometry as well as the downstream blood flow over time.

8 Conclusions

The present study investigated the interactions between the blood flow and artery geometry in a real model extracted from CT-Scan images of an Artery Bifurcation with Moderate arteriosclerosis. Results showed that employing Newtonian models for the blood flow does not lead to promising results at occluded areas and beyond them as well. It was also demonstrated that blood flow effects on the artery wall exist through the whole blood pulse cycle and are different in every phase. Wall displacement negligibly affected the geometry and had insignificant effects on larger arteries. However, in the studied geometry, the maximum displacement occurred after the occlusion, and its long-term effects on the real geometry were observable, causing vortices and disturbances to develop in the downstream area. The maximum shear stress created after the occlusion may cause damages to the artery endothelial cells by rupturing them.

Compliance with ethical standards

References

1. Heart disease and stroke statistics, American Heart Association, published online ahead of print 2014, Dallas, Texas, USA
2. ECDS (2016) British Heart Foundation of Health Promotion Research Group, http://www.heartstats.org/
3. 2016 Everyday Health Media, LLC (2016) http://www.everydayhealth.com/
4. American Heart Association (2016). http://www.heart.org/
5. Haghighi AR, Asadi Chalak S (2016) A non-Newtonian model of pulsatile blood flow through elastic artery with overlapping stenosis. Modarres Mechanical Engineering 16(3):232–238
6. Young DF (1968) dependent stenosis on flow through a -Effect of a time tube. Journal of Engineering for Industry 90(2):248–254
7. Lee J, Fung Y (1970) Flow in locally constricted tube at low Reynolds number. J Appl Mech 37(1):379–416
8. Morgan BE, Young DF (1974) An integral method for the analysis of flow in arterial stenosis. Bull Math Biol 36(1):39–53
9. Azuma T, Fukushima T (1976) Flow patterns in stenotic blood vessel models. Biorheology 13(6):337–355
10. Liu GT, Wang XJ, Ai BQ, Liu LG (2004) Numerical study of pulsating flow through a tapered artery with stenosis. Chin J Phys 42(4):401–409
11. Yamaguchi N (2005) Existence of global strong solution to the micropolar fluid system in a bounded domain. Mathematical Methods in the Applied Sciences 28(13):1507–1526
12. Cho YI, Kensey KR (1991) Effects of the non-Newtonian viscosity of blood on hemodynamic of diseased arterial flows: Part 1. Biorheolgy 28(3–4):241–262
13. Mandel PK (2005) An unsteady analysis of non-Newtonian blood flow through tapered arteries with a stenosis. International Journal of Non-Linear Mechanics 40(1):151–164
14. Obidowski D, Jozwik K (2010) Numerical simulation of the blood flow through vertebral arteries. J Biomech 43:177–185
15. Wang Y, Xie X, Zhou H (2013) Impact of coronary tortuosity on coronary blood flow: A 3D computational study. J Biomech 46:1833–1841
16. Jalali P, karimi S, Dabagh M, Vasava P, Dadvar M, Dabir B (2014) Effect of rheological models on the hemodynamics within human aorta: CFD study on CT image-based geometry. J Non-Newtonian Fluid Mech 207:42–52
17. Barrett KE, Barman SM, Boitano S, Brooks H (2015) Ganong's Review of medical physiology, 24th Edition (LANGE Basic Science), California, ISBN-13: 978–0071780032
18. Razavi A, Shirani E, Sadeghi MR (2011) Numerical simulation of blood pulsatile flow in a stenosed carotid artery using different rheological models. J Biomech 44:2021–2030
19. Sinnott MD, Cleary PW, Prakash M (2006), An investigation of pulsatile blood flow in a bifurcating artery using a grid-free method, *Fifth International Conference on CFD in the Process Industries CSIRO, Melbourne, Australia*
20. Chan WY (2007) Modeling of non-Newtonian blood flow through a stenosed artery incorporating fluid-structure interaction. ANZIAM J 47:507–523
21. Abdollahzadeh Jamalabadi MY, Daqiqshirazi M, Nasiri H, Safaei MR, Nguyen TK (2018) Modeling and analysis of biomagnetic blood Carreau fluid flow through a stenosis artery with magnetic heat transfer: A transient study. PLoS One 13(2):e0192138
22. Fry DL (1968) Acute vascular endothelial changes associated with increased blood velocity gradients. Circ Res 22:165–197
23. Ramstack JM, Zuckerman L, Mockros LF (1979) Shear induced activation of platelets. J Biomech 12:113–125